NASA TECHNICAL MEMORANDUM

NASA TM X-71623

NASA TM X-71623

STRUCTURAL RESPONSE OF A FIBER COMPOSITE COMPRESSOR FAN BLADE AIRFOIL

by C. C. Chamis and M. D. Minich
Lewis Research Center
Cleveland, Ohio 44135

TECHNICAL PAPER to be presented at
Gas Turbine Conference and Products Show
Houston, Texas, March 2-6, 1975

TABLE OF CONTENTS

E-8142

STRUCTURAL RESPONSE OF A FIBER COMPOSITE COMPRESSOR FAN BLADE AIRFOIL

By

C. C. Chamis* and M. D. Minich **

Lewis Research Center
National Aeronautics and
Space Administration
Cleveland, Ohio

Abstract

A theoretical investigation was performed to determine the structural response of a fiber composite airfoil typical of those encountered in high-tip speed compressor fan blades when subjected to load conditions anticipated in such applications. The analysis method used consists of composite mechanics embedded in pre- and post-processors and coupled with NASTRAN. The load conditions examined include thermal due to aerodynamic heating, pressure due to aerodynamic forces, centrifugal, and combinations of these loads. The various responses investigated include root reactions due to various load conditions, average composite and ply stresses, ply delaminations, and the fundamental modes and the corresponding reactions. The results show that the thermal and pressure stresses are negligible compared to those caused by the centrifugal forces. Also, the core-shell concept for composite blades is an inefficient design (core plies not highly stressed) and appears to be sensitive to interply delaminations. The results are presented in graphical and tabular forms to illustrate the types and amount of data required for an analysis such as this, and to provide quantitative data associated with the various responses which can be helpful in designing composite blades.

---

*Aerospace Engineer, Materials and Structures Division

**Associate Professor, Department of Civil Engineering, The Cleveland State University, Cleveland, Ohio

INTRODUCTION

The recent national awareness of the need to conserve our natural resources provides a strong motivation for efficient material utilization and the development of new design concepts for structural components in general. One particular area where efficient material utilization and new design concepts could help conserve natural resources is in the use of fiber composites in high-tip-speed airfoils for compressor fan blades in aircraft engines. Increasing the airfoil tip speed permits reduction of the number of stages in the compressor to attain a given thrust. By using advanced composites, higher airfoil tip speeds and lighter weights can be attained compared to the use of state-of-the-art materials. Both higher tip speed and lighter weight airfoils have an accumulative effect on reducing the amount of material used in an aircraft engine.

Advanced fiber composites application to high-tip-speed airfoils is currently under investigation by the NASA Lewis Research Center under contract NAS3-15335 with Pratt and Whitney Aircraft, East Hartford, Conneticut. Another application is reported in reference 1.

A computerized analysis capability which can be used to analyze fiber composite airfoils is described in reference 2, along with analysis results for a specific design. However, the structural response of composite airfoils due to various loading conditions has not been investigated.

Determining the structural response of the airfoil due to various loading conditions is useful in several respects. For example: (1) The airfoil stiffness and thermal properties may be used to obtain an a priori assessment of the deformation and stresses in the airfoil when subjected to various load

conditions. (2) The stresses, deflections, and root reactions produced by thermal, aerodynamic pressure and centrifugal loading conditions can be examined to determine which is the dominant loading condition. If a dominant loading condition is established, then only this loading condition need be used in preliminary designs, thereby saving considerable man-hours of effort and computer time. (3) Tip deflections due to combined loading may be studied in order to determine the need for offsetting unacceptable radial growth, uncambering and untwisting. (4) End reactions due to vibrations may be studied to determine whether high cycle fatigue may be a design problem at the root attachment.

The primary objective of this investigation is to use the computerized capability (ref. 2) to theoretically examine the structural response of a composite airfoil, typical of those encountered in high-tip-speed compressor fan blade applications. The airfoil is assumed to be subjected to the following loading conditions: thermal, dynamic pressure, centrifugal, a combination of these, and vibration. The structural response of interest includes: airfoil stiffness and thermal properties, displacements, composite and ply stresses, root reactions, through-the-thickness shear forces and stresses, interply delamination, airfoil fundamental frequencies and their respective root reactions. The centrifugal load stiffening effects and vibration mode shapes are extensively discussed in reference 2 and, therefore, are considered in this investigation only briefly. A secondary objective is to provide quantitative guide data for designing airfoils for high-tip-speed compressor blade applications.

The airfoil geometry, aerodynamic loads, and rotational speed selected are representative of the preliminary design of a high-tip-speed blade, and

were obtained from the contract previously mentioned. The laminate configuration is of the core-shell type: 0° plies for the core and $\pm 45°$ plies for the shell. Briefly this capability consists of composite micromechanics, macromechanics, and laminate analysis embedded in pre- and post-processors and coupled with NASTRAN.

INPUT DATA

The input data for the computerized analysis consists of the following items:

1. Airfoil geometry defined at several cross sections along the airfoil span
2. Airfoil operating temperature
3. Airfoil dynamic pressure difference between pressure and suction surfaces
4. Composite system
5. Airfoil laminate configuration, i.e. number of plies and ply orientation
6. Finite element representation including load case selection, type of solution (static, dynamic) and boundary conditions.

For the specific blade under consideration, the airfoil geometry was specified as input at three cross sections: root, midspan and tip. The airfoil operating temperature and pressure difference were specified as input at the same sections for convenience. Pertinent data, obtained from the contract previously mentioned, are summarized in Table 1 which is a computer output of the input data.

The composite system selected was Modmor II (Mod-II)graphite/PMR polyimide. The ply thickness used was 0.007 inches at 0.57 fiber volume ratio and zero voids. The laminate configuration for the airfoil was of the core-shell version, symmetric about the midplane. The ply orientation was as follows: 60 percent of the plies at the airfoil maximum thickness were oriented at 0° (core plies) and the remaining 40 percent were at $\pm 45°$ (shell plies). The 0° direction is parallel to the span or radial direction. These input data are summarized in Table 2 which is a computer output of the composite type and ply geometry. In Table 2 the ply starting (%I) and stopping (%F) points (ply contours) are given as distance percentages along the coordinate axes of the airfoil. See also Nomenclature. Note the type of format in Table 2 was selected to accomodate usage of hybrids in both the same ply level and through the thickness. This type of format also accomodates specification of positioning of leading edge devices.

The last part of the data input is the finite element representation of the airfoil under consideration, the boundary conditions and data to specify additional loading conditions. A photograph of the airfoil looking down on the tip is shown in figure 1. The finite element representation of the airfoil is shown in figure 2 where both the nodal (grid) points and the elements are defined by numbers. The element numbers are in parenthesis to differentiate them from the numbers defining grid points. Note that the airfoil projected plane has an aspect ratio (span/chord) of approximately one. The finite element used is triangular, plane stress, anisotropic, and accomodates both bending and stretching. It is defined as element CTRIA2 in the NASTRAN L15.5 library of elements. The boundary conditions specified consist of fixing the three translations (displacements along x, y and z coordinate

directions) and the three rotations (slopes about the x, y and z coordinated directions) along the root (grid points 1 through 9, figure 2). The rotation about z is fixed at all grid points because of the relatively shallow camber of the airfoil, see figure 1. All other translations and rotations are free. Three additional inputs for loading conditions consist of: the airfoil rotational speed (250 revolutions per second, 2200 feet per second tip speed), the lamination temperature difference (-530°F), and the combined temperature loading (operating temperature - lamination temperature).

AIRFOIL INTERPOLATED DATA

The input data described in the previous section is operated on by the pre-processor (reference 2) to generate the following data:

1. Coordinates of grid points
2. Airfoil temperature at the grid points
3. Airfoil pressure difference at the grid points
4. Airfoil thickness at the grid points
5. Ply number and stacking sequence at the grid points

The data generated for items (1) to (5) above are in the form of internal tables (arrays) and are used as inputs by the pre-processor for subsequent operations. These data are also printed out in table form. Herein, the data generated for items (2) to (5) above are presented as contour plots in figures (3) to (6) in order to illustrate graphically their span-wise (root-tip) and chord-wise (leading edge-trailing edge) variations. Note that in figure 6 two numbers are given for each ply contour. The first number denotes the total number of plies while the second number in parentheses denotes the number of plies at 0°. Note, furthermore, the concentration of 0° plies in

the airfoil midchord region. Note also the similarity between ply contours (figure 6) and thickness contours (figure 5), as is expected.

AIRFOIL STIFFNESS AND THERMAL PROPERTIES

The stiffness and thermal properties of the airfoil required for the finite element analysis constitute part of the airfoil structural response and are generated via the pre-processor (reference 2). The various airfoil stiffness and thermal properties generated along the x, y, z coordinates of the airfoil, figure 2, are the following:

1. Moduli and Poisson's ratio
2. Thermal coefficients of expansion
3. Membrane stiffnesses
4. Bending stiffnesses
5. Thermal forces
6. Plane-stress stress-strain and temperature relationships compatible with the CTRIA2 NASTRAN finite element.

The above properties are plotted in figures (7) to (14) to illustrate graphically their span-wise and chord-wise variations. The format in these figures is as follows. The properties are plotted along the chord at three span sections: root, midspan and tip. These are noted, respectively, by R, M, and T on the curves. The properties along the chord are plotted at the leading edge (noted L.E. on the curve), trailing edge (noted T.E. on the curve) and equidistant intermediate points (chord-fractions).

Considerable insight on how the airfoil will respond when subjected to mechanical and/or thermal loads may be obtained by studying the properties plotted in figures (7) to (12). For example, in figure 7a, it is seen that

the modulus in the span direction is about twice as high at midchord than it is at the two edges. The converse is true for the in-plane shear modulus, figure 7c. Also the major Poisson's ratio is higher at the edges than it is at midchord and is large (greater than .60) when compared to homogeneous isotropic elastic materials (about .30). These large Poisson's ratio values result from the dominance of the $\pm 45°$ plies at the edges.

The thermal coefficient of expansion in the span direction, figure 8a, is negative at midchord and positive at the edges and is relatively small compared to structural metals. Because the coefficient is smaller in the midchord region than at the edges, increasing temperature will subject this airfoil to compression forces at the edges and tensile forces at midchord. The opposite effect will occur in the chord direction, figure 8b, since this coefficient of expansion is higher at midchord than it is at the edges.

The membrane stiffness in the span direction (A_{c11}), figure 9a, is greater at midchord than it is at the edges. This means that an applied load in the span direction, such as the centrifugal, will be carried mainly by the blade midchord region. This is so because there is a concentration of 0° plies in this region (figure 6).

The bending stiffness in the span direction (D_{c11}), figure 10a, shows similar variation as the membrane stiffness (A_{c11}). This will cause the bending loads along the span to be carried primarily by the midchord portion of the airfoil. Note the variation of the bending stiffness in the chord direction (figure 10c) and the torsional stiffness (figure 10d). Both of these are considerably lower near the edges than they are at the midchord region. Airfoils with stiffness distributions as shown in figures 10c and 10d are susceptible to low frequency chordwise and torsional vibrations at

the edge regions and particularly near the tip.

Airfoils made from angleplied laminates will possess bending-twisting coupling. The distribution of stiffnesses which produce bending-twisting coupling are illustrated in figure 11. The magnitudes of the coupled stiffnesses in figure 11 are considerably smaller than those in figure 10. Airfoils possessing coupling stiffnesses when subjected to bending loads will also twist. Airfoils with material coupling will vibrate in complex modes and not in the decoupled modes first bending, second bending, or first torsional as is generally considered to be the case with airfoils made from homogeneous isotropic materials.

The distribution of the thermal forces is shown in figure 12. Note the sense of these forces is consistent with that mentioned in the discussion of the thermal coefficients of expansion, figure 8. The variation of the plane-stress stress-strain coefficients and the plane-stress thermal coefficients of expansion compatible with the CTRIA2 NASTRAN finite element are shown in figures 13 and 14 respectively. Note the variations of the thermal coefficients in figures 14a and 14b are different from those in figure 8a and 8b because the former are evaluated at the element center while the latter at the node. Note also in figure 14c that the coefficient (α_{12}) will produce shearing with changes in airfoil temperature. This shearing is caused by the presence of the in-plane stretching-shearing coupling coefficients (figures 13e and 13f). As a side note, the NASTRAN CTRIA2 plate element permits bending-twisting coupling via the moment-area integrals of the nonsymmetric terms G_{13} and G_{23} in the stress-strain relationships.

AIRFOIL RESPONSE FROM VARIOUS LOADING CONDITIONS

The airfoil under consideration was subjected to the various load conditions listed in Table 3. The response from these load conditions consists of: root reactions, displacements, composite surface stresses, through the thickness shear forces, maximum stressed ply stresses, interply delamination, and margins of safety. These responses were determined using the analysis capability described in reference 2 and are discussed in detail in the sections that follow.

Root Reactions

The force root reactions are presented graphically in figure 15. Note in this figure that the reaction forces due to centrifugal forces dominate those from the other loading conditions. The magnitudes of these reaction forces are used to design the airfoil root attachment. Note the high magnitude of F_z near the trailing edge, figure 15c. This indicates that forces which tend to untwist the airfoil are set up.

Corresponding plots for the root reaction moments are shown in figure 16. The reaction moments due to centrifugal force dominate those from the other loading conditions.

Airfoil Tip Displacements

The airfoil tip displacements due to the various loading conditions examined are presented graphically in figure 17. Note the scale for the ordinates in this figure are irregular; however, the scale varies linearly between the minimum and maximum values. The displacement in the span

direction indicates radial growth, in the chord direction, uncambering, and in the z-direction (thickness direction, approximately) out-of-plane bending and twisting.

The results in figure 17 are useful in determining pre-twist, pre-camber and pre-tilt in order to keep the resulting displacements within design tolerance requirements. Note the tip displacements due to centrifugal load dominate those from the other loading conditions. Note also that the chord direction and "bending" tip displacements due to pressure are in the opposite direction as compared with those due to centrifugal load. Furthermore, those due to thermal load are negligible compared to those from the other loading conditions.

Composite Surface Stresses

The composite surface stress in the span direction (σ_{cxx}) is presented graphically in figures 18 (pressure surface) and 19 (suction surface). In these figures, the σ_{cxx} variation due to various loading conditions is shown along the chord at three sections along the span: root (R), midspan (M), and tip (T). The following are observed from figures 18 and 19:

1. The thermal stress is negligible compared to that from the centrifugal loading.
2. The pressure stress is about 20 percent of the centrifugal stress.
3. The stress σ_{cxx} reaches its maximum magnitude (125 ksi) on the pressure surface at the root near the leading edge, figure 18d.
4. The stress σ_{cxx} has minimum magnitude (60 ksi) at midspan in the midchord region (figure 19d).

The variation of the composite surface stress in the chord direction (σ_{cyy}) is presented graphically in figures 20 (pressure surface) and 21 (suction surface). The maximum magnitude of this stress (100 ksi) is on the pressure surface at the leading edge in the root, figure 20d. Everywhere else the magnitude is less than 20 ksi. The high magnitude of 100 ksi is also caused in part by the specification of the boundary conditions. Allowing the airfoil to move along the root chord near the leading edge will decrease this magnitude substantially.

The variation of the composite surface shear stress (σ_{cxy}) on the pressure surface due to various loading conditions is presented graphically in figure 22. The corresponding variation on the suction surface is presented in figure 23. The following are observed from the results in figures 22 and 23:

1. The shear stress due to centrifugal load is the dominant stress.
2. The pressure surface shear stress (figure 22) has a maximum magnitude (60 ksi) in the leading edge near the root and a minimum magnitude (-40 ksi) in the leading edge at the midspan region.
3. The suction surface shear stress (figure 23) has a maximum magnitude (30 ksi) in the leading edge at the root and a minimum magnitude (15 ksi) in the trailing edge at the midspan region.
4. The shear stress has the same sign in the leading edge on both the pressure and suction surface. Similarly, the sign is the same in the trailing edge. This indicates that the airfoil is undergoing untwisting.

Through-the-Thickness Shear Forces

The variation of the shear force (Q_{xz}) through the airfoil thickness on a section normal to the span due to various loading conditions is presented graphically in figure 24. As can be seen in this figure, the dominant shear force is that due to the centrifugal load. The combined shear force has a maximum magnitude of 2000 pounds/inch in the midchord region at the root, figure 24d. The maximum shear stress due to this force is given by the formula $1.5Q_{xz}/t$ where t is the airfoil thickness at that section. Using 2000 pounds/inch for Q_{xz} and 0.5 inch for t yields a maximum shear stress of 6000 psi. This value is about 40 percent of interlaminar shear strength as determined by the short beam shear test for the composite system used in the airfoil under consideration.

The corresponding variation of the shear force (Q_{yz}) through the thickness on a section normal to the chord is shown in figure 25. The maximum shear stress corresponding to the maximum shear force, figure 25d, is 7800 psi. Since both Q_{xz} and Q_{yz} cause stresses which are maximum at the same plane, they could cause delamination, similar to that observed in a short-beam-shear (interlaminar shear) test.

MAXIMUM-STRESSED-PLY STRESSES

The most effective way to assess the adequacy of an airfoil laminate configuration with respect to stress is at the ply level. This is because the combination of $\pm 45°$ and 0° plies varies considerably throughout the airfoil and a large number of laminates need to be tested, at combined loads, if the assessment is to be made at the laminate level.

Combined Loading at Operating Temperature

For the airfoil under consideration the ply stresses of the maximum-stressed-ply due to combined load (without residual stress) are summarized in Table 4. Data are compiled for several chord fractions near the root, midspan, and near the tip sections. Refering to figure 2, these are respectively: nodes 10-18, 37-45, and 64-72. Table 4 contains the following information:

1. Span section and chord-fraction first column
2. Number of plies at chord-fraction, second column
3. Maximum stressed ply, third column
4. Ply stress: along fiber ($\sigma_{\ell 11}$), transverse to fiber ($\sigma_{\ell 22}$) and intralaminar stress ($\sigma_{\ell 12}$)
5. Ply combined-stress margin of safety (MOS) based on modified distortion energy principle refs. 3, 4, or 5, column 7
6. The last three columns have information with respect to interply delamination: adjacent plies, angle change ($\Delta\theta$) and margin of safety (MOS) (ref. 5), respectively.
7. Unidirectional composite fracture stresses at the bottom of the table from which the ply MOS is calculated as discussed in refs. 3, 4, or 5.

Note negative MOS is Tables 4 and 5 denote ply failure, and thus a critically stressed ply. The following are observed from the results in Table 4:

1. The maximum stressed plies are within the shell; the shell includes the first 14 plies, and the last 14 plies at the maximum blade thickness.

2. Negative MOS's are indicated in plies in the leading and trailing edges at the root and midspan and in the trailing edge at the tip. Comparing the individual ply stresses with the unidirectional composite fracture stresses it is seen that the negative MOS is caused primarily by either high intralaminar shear stress or high transverse stress in all cases except in the trailing edge at midspan. At this latter point the negative MOS is caused by high longitudinal compressive stress.
3. The core (0°) plies carry less load compared to shell (±45°) plies at the same chord fraction since the high stressed plies are in the shell. Though detail data are not presented here, the $\sigma_{\ell 11}$ stress magnitudes in the core plies are less than 75 percent of those in the maximum-stressed shell plies and in many cases less than 50 percent. Therefore the core plies are used inefficiently in this airfoil laminate configuration.
4. Interply delamination or near delamination (MOS $\simeq$ 0) is indicated in adjacent plies within the shell and in adjacent plies between shell and core. This means that the core-shell laminate configuration for airfoils in general may be susceptible to interply delamination.

Lamination Residual Stress

The ply stresses of the maximum-stressed-ply due to lamination residual stress is induced by the temperature difference between cure and room temperatures (-530°F). The ply stresses from this source are summarized in Table 5. The following are observed from these results:

1. The maximum stressed plies are within the shell.
2. Negative MOS's are indicated along the trailing edge. In all cases this is due primarily to a high transverse tensile stress. At the midspan and tip section, there is also a high longitudinal compressive stress.
3. Interply delamination or near delamination (MOS $\simeq$ 0) is indicated within the shell. This means that this laminate configuration is susceptible to transverse ply (transply) cracking and interply delamination at these locations after molding but without additional loading.

Combined Loading with Residual Thermal Stresses at Operational Conditions

The temperature load condition for this case was obtained by using the operational temperature (figure 3) minus the lamination temperature (600°F). It is a combined case with the pressure and centrifugal forces also acting. This case, therefore, will include the ply residual stresses at the operational temperature and the stresses due to operating conditions. The ply stresses of the maximum-stressed-ply due to combined stresses are summarized in Table 6. The following are observed from these results:

1. The maximum stressed plies are within the shell.
2. Negative MOS's are indicated along the leading edge at the root and midspan section and all along the trailing edge. The negative MOS is caused primarily by intralaminar shear or high transverse tensile stress except at the trailing edge of the midspan section. At this point, the negative MOS is caused by high longitudinal compressive stress.

Note that the difference between the data in Table 6 and that in Table 4 is the ply residual stresses at operating conditions. Up to this point the results presented and discussed are based on a particular airfoil laminate configuration. However the data generated can be used to modify the laminate configuration for more efficient composite material utilization.

AIRFOIL VIBRATION

The vibrating of the airfoil under consideration was determined at zero-speed (no centrifugal force). The first 9 fundamental modes in cycles per second (CPS) are listed in ascending order in Table 7. As can be seen in this table the magnitude of the fundamental frequencies ranges from 234 CPS to 2495 CPS.

The reaction forces at the root due to first four fundamental frequencies are presented graphically in figure 26. As can be seen in figure 26, the reaction forces are of cyclic nature ranging from: -8000 to 7000 pounds for F_x, -3000 to 4500 pounds for F_y, and -1500 to 3000 pounds for F_z. These magnitudes are comparable to those of the root reaction forces due to centrifugal load, figure 15. The vibration reaction forces are in the high cycle fatigue regime and could produce difficulties if the root attachment is not designed to accomodate these cyclic loads.

SUMMARY OF RESULTS AND CONCLUSIONS

The major results and conclusions of an investigation to theoretically examine the structural response of composite airfoils for high-tip-speed compressor fan blades for aircraft turbine engines subjected to various

loading conditions (thermal, pressure, centrifugal, and combinations of these) are as follows:

1. The root reactions, tip displacements and composite stresses due to thermal and pressure loading conditions are negligible compared to those produced by the centrifugal loading.
2. The combined loading condition produced high stresses in the shell plies of the core-shell airfoil laminate configuration (0° core, $\pm$45° shell) considered. These high stresses could produce ply failure in the shell plies in the leading and trailing edge regions at the root and midspan sections, and in the trailing edge at the tip section.
3. The core plies carry less load compared to shell plies resulting in inefficient use of the core plies in the core-shell type of configuration.
4. The combined loading case could produce interply delamination due to relative rotation in adjacent plies in the shell and between shell and core at the midchord and in the leading and trailing edge regions at the root and midspan sections.
5. The combined loading case produced high through-the-thickness shear stresses at the midchord in the root section. These stresses have sufficiently high magnitudes to produce interply delamination similar to that observed in short-beam-shear (interlaminar shear) tests.
6. The root reactions due to various vibration modes are cyclic and are comparable to those of the combined load case. These reactions may subject the root attachment to high cycle fatigue.

7. The stiffness and thermal properties of the airfoil section may be used to obtain an a priori assessment of the airfoil structural response.
8. The core-shell type of laminate configuration for airfoils for high-tip-speed compressor fan blade applications appears to be inefficient with respect to high ply stresses near the edges and interply delamination between shell and core.
9. The lamination residual stresses in the plies at room temperature could produce ply failure (transply cracks) and interply delamination in the shell plies along the trailing edge. These failures are caused primarily by high transverse and intralaminar shear stresses.
10. The combined loading at operational temperature causes ply failure in the shell plies along both the leading and trailing edges. These failures are caused primarily by high transverse and intralaminar shear stresses.
11. The results presented herein may be used as a guide for high-tip-speed airfoil designs using composites with respect to: stiffness, thermal loads, root reactions, composite and ply stresses, tip displacements and fundamental frequencies.
12. Preliminary designs for high-tip-speed composite airfoils for sufficient strength and minimum tip displacements may be based only on the centrifugal load since the structural response from this load dominates all the other loading conditions.

REFERENCES

1. Hanson, M. P., Chamis, C. C.: Graphite - Polymide Composite for Application to Aircraft Engines. NASA TN D - 7698, 1974.

2. Chamis, C. C., Lynch, J. E. : High-Tip-Speed Fiber Composite Compressor Blades Vibration and Strength Analysis. NASA TMX - 71589, 1974.

3. Chamis, C. C.: Failure Criteria for Filamentary Composites. NASA TN D - 5367, 1969.

4. Chamis, C. C.: Failure Criteria for Filamentary Composites, Composite Materials: Testing and Design, ASTM STP 460, American Society for Testing and Materials, 1969, pp. 336-351.

5. Chamis, C. C.: Computer Code for the Analysis of Multilayered Fiber Composites - Users Manual. NASA TN D - 7013, 1971.

NOMENCLATURE

A_c	axial stiffness array-position denoted by numerical subscription
$C_{,c}$	subscript - composite property
D_c	bending stiffness array - position denoted by numerical subscripts
F	reaction force - direction denoted by subscript; terminal point of ply-type
FVR	fiber volume ratio
G	array of anisotropic stress-strain relationships for the NASTRAN plate elements - position denoted by numerical subscripts
I	starting point of ply-type
L.E.	leading edge of airfoil subscript - ply property
M	midspan section; moment-direction denoted by numerical subscripts
MOS	margin of safety
P	pressure
Q	shear force through airfoil thickness-surface and direction denoted by subscripts
R	root section
T	temperature
T.E.	trailing edge of airfoil
t	airfoil thickness
VVR	void volume ratio
x,y,z	airfoil structural axes, x-along span; y-along chord; z-along thickness, subscripts -- corresponding coordinate directions
1,2,3	subscripts - array position or ply principal direction with "1" along fiber
ZL	Z - coordinate to pressure surface
ZU	Z - coordinate to suction surface
α	thermal coefficient of expansion-direction denoted by numerical subscript

$\Delta\theta$ interply relative rotation

σ stress-type and direction denoted by subscripts

TABLE 1 INPUT DATA BLADE GEOMETRY, TEMPERATURE AND PRESSURE

SECTION	X RADIUS	Y CHORD	ZU SUCTION SURFACE	ZL PRESSURE SURFACE	T TEMPERATURE	DELTA-P PRESSURE DIFFERENCE
1	9.38	.000	.060	.000	181.	10.5
1	9.38	1.00	.500	.200	175.	10.0
1	9.38	2.00	.800	.400	190.	9.00
1	9.38	3.00	.955	.440	205.	7.00
1	9.38	4.00	.910	.404	212.	5.50
1	9.38	5.00	.770	.310	220.	4.50
1	9.38	6.00	.350	.121	227.	4.00
1	9.38	6.60	.062	.000	235.	3.50
2	13.0	-.150	-.900	-.950	285.	14.5
2	13.0	.000	-.850	-.900	275.	14.5
2	13.0	1.00	-.400	-.550	265.	12.5
2	13.0	2.00	.050	-.200	275.	9.50
2	13.0	3.00	.650	.200	285.	7.50
2	13.0	4.00	1.05	.590	287.	6.00
2	13.0	5.00	1.35	.980	289.	6.00
2	13.0	6.00	1.55	1.40	292.	7.00
2	13.0	6.65	1.75	1.70	296.	7.20
3	16.4	-.300	-1.31	-1.35	443.	15.0
3	16.4	.000	-1.20	-1.25	415.	14.0
3	16.4	1.00	-.700	-.773	386.	13.0
3	16.4	2.00	-.150	-.350	386.	10.0
3	16.4	3.00	.450	.050	386.	7.00
3	16.4	4.00	1.00	.650	386.	8.00
3	16.4	5.00	1.50	1.30	386.	12.0
3	16.4	6.00	2.17	2.07	386.	14.0
3	16.4	6.50	2.50	2.45	388.	12.0

NOTE: Dimensions are as follows:

Distance Inches

Temperature °F

Pressure PSI

TABLE 2 INPUT DATA OF COMPOSITE TYPE AND PLY GEOMETRY

%I	THICKNESS %F	PLY ORIENT	DESIG-NATION	X-COORDINATE %I	%F	Y-COORDINATE %I	%F	TYPE OF COMP. FIBER/MATRIX		PLY THICKNESS	PLY VVR	PLY FVR
0.0	20.0	45.0	1.0	.0	100.1	.0	100.1	MOD2	POLY	.007	.000	.570
20.0	50.1	.0	2.0	.0	100.1	.0	100.1	MOD2	POLY	.007	.000	.570

%I Starting point of ply-type

%F Terminal point of ply-type

VVR Void Volume Ratio

FVR Fiber Volume Ratio

TABLE 3 SUMMARY OF CASES EXAMINED

CASE	DESCRIPTION
1	THERMAL LOAD ONLY
2	PRESSURE LOAD ONLY
3	CENTRIFUGAL FORCE ONLY
4	COMBINED , CASES 1-3
5	RESIDUAL STRESS
6	OPERATING THERMAL STRESS
7	VIBRATION MODES

TABLE 4 MAXIMUM-STRESSED-PLY STRESSES AT SELECTED CROSS SECTIONS DUE TO COMBINED LOADING

	CHORD FRACTION		PLIES PER NODE	MAX. STRESSED PLY	PLY STRESSES (KSI) $\sigma_{\ell 11}$	$\sigma_{\ell 22}$	$\sigma_{\ell 12}$	COMB.STRESS MOS	PLY RELATIVE ROTATION ADJ. PLIES	$\Delta\theta$ DEG	COMB.STRESS MOS
A.	ROOT SECTION:	L.E.	7	7	- 96.4	- 30.1	8.2	- 23.	6/7	-.025	-2.93
		1/8	30	30	15.8	- 3.1	16.2	.081	16/17	.0052	.190
		1/4	45	45	65.3	- 1.4	12.4	.299	31/32	.0051	.206
		3/8	58	58	114.	- .2	9.4	.246	51/52	-.0064	.012
		1/2	71	71	103.	~ 0	3.4	.592	70/71	-.0059	.092
		5/8	70	2	56.4	- 1.3	- 1.6	.845	1/2	.0046	.295
		3/4	64	63	31.4	- 2.1	.9	.924	62/63	.0039	.395
		7/8	37	15	21.2	- 4.0	.1	.904	35/36	.0034	.467
		T.E.	8	1	31.4	- 8.2	- 36.3	- 3.66	2/3	-.0067	- .039
B.	MID - SPAN : SECTION	L.E.	6	1	-159.3	- 5.3	- 22.6	- 1.52	1/2	.0086	- .331
		1/8	16	1	- 51.6	- 3.3	- 8.9	.667	1/2	.0052	.204
		1/4	27	27	78.1	- 1.0	3.1	.723	26/27	-.0054	.163
		3/8	42	42	108.2	- .9	1.6	.545	35/36	-.0063	.024
		1/2	60	60	87.1	- .7	~ 0	.711	59/60	-.0056	.131
		5/8	61	47	67.1	- 2.7	- .5	.751	59/60	.0042	.356
		3/4	51	37	56.5	- 4.1	- .2	.749	2/3	-.0042	.343
		7/8	26	25	34.0	- 2.0	8.5	.680	2/3	-.0050	.235
		T.E.	6	2	-241.8	- 6.5	7.1	- 1.21	2/3	-.0095	- .465

TABLE 4 CONTINUED

	CHORD FRACTION		PLIES PER NODE	MAX. STRESSED PLY	PLY STRESSES (KSI)				PLY RELATIVE ROTATION		
					$\sigma_{\ell 11}$	$\sigma_{\ell 22}$	$\sigma_{\ell 12}$	COMB.STRESS MOS	ADJ. PLIES	$\Delta\theta$ DEG	COMB.STRESS MOS
C.	TIP SECTION:	L.E.	5	2	24.9	- 4.6	3.0	.842	1/2	.0062	.049
		1/8	8	8	- 2.3	- 4.8	- 4.6	.871	1/2	.0049	.250
		1/4	17	17	2.7	- 4.3	- 5.5	.845	16/17	-.0046	.296
		3/8	33	19	32.8	- 5.2	- .4	.819	32/33	-.0049	.247
		1/2	51	37	16.4	- 4.8	.6	.894	50/51	-.0051	.215
		5/8	48	34	25.8	- 4.8	- 0	.863	47/48	-.0040	.383
		3/4	33	19	36.0	- 5.2	.3	.802	32/33	-.0049	.245
		7/8	17	17	32.5	- 3.8	- 8.8	.614	16/17	-.0058	.110
		T.E.	5	5	85.0	- .4	- 34.4	- 3.181	4/5	-.0053	.188

NOTES: Unidirectional Composite

Material Fracture Stresses

Longitudinal Tensile	170 KSI
Longitudinal Compression	150 KSI
Transverse Tensile	9 KSI
Transverse Compression	20 KSI
Intralaminar Shear	17 KSI

Interply Delamination
Critical Angle $\Delta\theta \approx$ .0065 DEG

TABLE 5 MAXIMUM-STRESSED-PLY STRESSES AT SELECTED CROSS SECTIONS DUE TO LAMINATION RESIDUAL STRESS

	CHORD FRACTION		PLIES PER NODE	MAX. STRESSED PLY	PLY STRESSES (KSI)				PLY RELATIVE ROTATION		
					$\sigma_{\ell 11}$	$\sigma_{\ell 22}$	$\sigma_{\ell 12}$	COMB. STRESS MOS	ADJ. PLIES	$\Delta\theta$ DEG	COMB. STRESS MOS
A.	ROOT SECTION:	L.E.	7	6	1.37	6.06	- 2.61	.578	1/2	-.0062	.034
		1/8	30	16	- 8.61	5.98	.02	.552	1/2	-.0059	.082
		1/4	45	31	- 4.95	6.04	.00	.568	43/44	-.0059	.083
		3/8	58	44	- 3.81	6.08	- .01	.568	2/3	.0059	.073
		1/2	71	15	- 4.15	5.94	- .02	.586	69/70	-.0059	.079
		5/8	70	15	- 5.52	6.11	.11	.555	68/69	-.0061	.061
		3/4	64	15	- 5.75	6.08	.04	.558	62/63	-.0059	.077
		7/8	37	15	- 7.44	5.99	.00	.559	2/3	.0059	.084
		T.E.	8	8	- 36.0	227.8	.98	-580.0	7/8	.2357	-35.4
B.	MID - SPAN SECTION:	L.E.	6	1	- 4.14	5.66	.00	.623	2/3	.0060	.067
		1/8	16	1	- 3.06	5.63	- .04	.633	2/3	.0059	.082
		1/4	27	27	- 2.65	5.64	- .08	.634	26/27	.0059	.084
		3/8	42	15	- 3.18	5.66	.00	.628	41/42	.0059	.082
		1/2	60	15	- 3.04	5.67	.00	.628	1/2	-.0059	.084
		5/8	61	47	- 3.29	5.66	.00	.627	1/2	-.0059	.082
		3/4	51	2	- 3.00	5.62	.07	.634	1/2	-.0059	.084
		7/8	26	2	- 3.02	5.63	.25	.633	1/2	-.0059	.082
		T.E.	6	6	-259.7	504.8	1.88	-2900	5/6	.5325	-81.21

TABLE 5 CONTINUED

	CHORD FRACTION		PLIES PER NODE	MAX. STRESSED PLY	PLY STRESSES (KSI)				PLY RELATIVE ROTATION		
					$\sigma_{\ell 11}$	$\sigma_{\ell 22}$	$\sigma_{\ell 12}$	COMB.STRESS MOS	ADJ. PLIES	$\Delta\theta$ DEG	COMB.STRESS MOS
C.	TIP SECTION:	L.E.	5	1	- 2.60	5.63	- .09	.636	2/3	.0059	.086
		1/8	8	2	- 2.68	5.63	.02	.635	1/2	-.0059	.084
		1/4	17	1	- 2.75	5.62	.03	.636	2/3	.0059	.086
		3/8	33	15	- 3.41	5.63	.01	.630	2/3	.0059	.084
		1/2	51	15	- 3.05	5.63	.00	.632	2/3	.0059	.086
		5/8	48	15	- 2.91	5.61	.00	.635	1/2	-.0059	.086
		3/4	33	1	- 3.07	5.61	- .03	.635	2/3	.0059	.084
		7/8	17	1	- 2.99	5.63	- .08	.634	2/3	.0059	.083
		T.E.	5	5	-101.1	218.5	- .13	-550.	4/5	.2299	-34.49

NOTES: Unidirectional Composite

Material Fracture Stresses

Longitudinal Tensile	170 KSI
Longitudinal Compression	150 KSI
Transverse Tensile	9 KSI
Transverse Compression	20 KSI
Intralaminar Shear	17 KSI

Interply Delamination
Critical Angle $\Delta\theta \approx .0065$ DEG

TABLE 6 MAXIMUM-STRESSED-PLY STRESSES AT SELECTED CROSS-SECTIONS DUE TO COMBINED THERMAL LOADING
(THERMAL LOADING = OPERATING TEMP. - LAMINATION TEMP.)

	CHORD FRACTION		PLIES PER NODE	MAX. STRESSED PLY	PLY STRESSES (KSI)				PLY RELATIVE ROTATION		
					$\sigma_{\ell 11}$	$\sigma_{\ell 22}$	$\sigma_{\ell 12}$	COMB. STRESS MOS	ADJ. PLIES	$\Delta\theta$ DEG	COMB. STRESS MOS
A.	ROOT SECTION:	L.E.	7	7	- 89.6	- 24.1	85.4	-24.0	2/3	.0013	.787
		1/8	30	16	- 67.0	9.12	.91	- .702	28/29	-.0057	.120
		1/4	45	31	- 61.9	10.2	1.61	- .929	41/42	-.0064	.009
		3/8	58	44	- 32.6	10.9	2.56	- .721	13/14	-.0053	.177
		1/2	71	57	17.2	8.57	1.97	.285	61/62	-.0064	.015
		5/8	70	15	13.2	6.11	- 1.23	.642	2/3	.0052	.195
		3/4	64	64	6.77	4.83	- .60	.766	63/64	.0046	.294
		7/8	37	37	- 8.69	3.49	- .62	.832	36/37	.0041	.372
		T.E.	8	1	17.5	- 3.25	-31.2	- 2.27	3/4	-.0053	.183
B.	MID - SPAN SECTION:	L.E.	6	1	-163.4	.31	-22.6	- 1.97	5/6	.0037	.429
		1/8	16	1	- 54.6	2.36	- 8.93	.417	2/3	.0050	.225
		1/4	27	1	- 40.1	2.64	- 7.75	.551	25/26	-.0052	.204
		3/8	42	41	20.6	7.57	- 1.45	.473	38/39	-.0064	.017
		1/2	60	59	84.3	4.94	.00	.636	58/59	-.0052	.202
		5/8	61	61	28.3	5.22	- 3.60	.748	60/61	.0038	.420
		3/4	51	51	13.0	4.12	- 4.25	.791	1/2	-.0038	.408
		7/8	26	26	15.5	4.35	- 8.75	.585	1/2	-.0045	.297
		T.E.	6	2	-250.	- .88	9.06	- 2.06	2/3	-.0036	.435

TABLE 6 CONTINUED

	CHORD FRACTION		PLIES PER NODE	MAX. STRESSED PLY	PLY STRESSES (KSI)				PLY RELATIVE ROTATION		
					$\sigma_{\ell 11}$	$\sigma_{\ell 22}$	$\sigma_{\ell 12}$	COMB.STRESS MOS	ADJ. PLIES	$\Delta\theta$ DEG	COMB.STRESS MOS
C.	TIP SECTION:	L.E.	5	1	- 20.2	2.97	- 3.08	.796	2/3	-.0022	.654
		1/8	8	1	- 2.53	2.90	- 3.29	.864	2/3	.0026	.604
		1/4	17	16	- 12.2	1.79	5.25	.846	15/16	-.0025	.609
		3/8	33	32	8.80	1.52	- 3.72	.879	19/20	-.0028	.560
		1/2	51	50	- 16.0	2.04	1.64	.903	49/50	-.0030	.537
		5/8	48	48	1.01	1.92	- 2.81	.935	34/35	-.0022	.660
		3/4	33	32	- 5.39	2.40	5.68	.816	19/20	-.0030	.528
		7/8	17	16	- 7.46	2.98	8.40	.646	15/16	-.0035	.463
		T.E.	5	5	82.0	5.24	-34.6	- 3.13	3/4	-.0028	.570

NOTES: Unidirectional Composite

Material Fracture Stresses

Longitudinal Tensile	170 KSI
Longitudinal Compression	150 KSI
Transverse Tensile	9 KSI
Transverse Compression	20 KSI
Intralaminar Shear	17 KSI
Interply Delamination Critical Angle $\Delta\theta$	$\approx$ .0065 DEG

TABLE 7 FUNDAMENTAL FREQUENCIES OF AIRFOIL AT ZERO SPEED

MODE	FREQUENCY CYCLES/SECOND
1	234
2	736
3	903
4	1326
5	1526
6	1827
7	1998
8	2350
9	2495

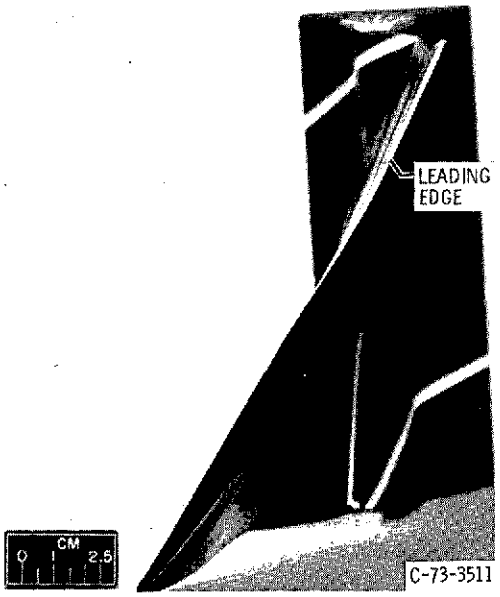

Figure 1. - Airfoil showing camber and twist.

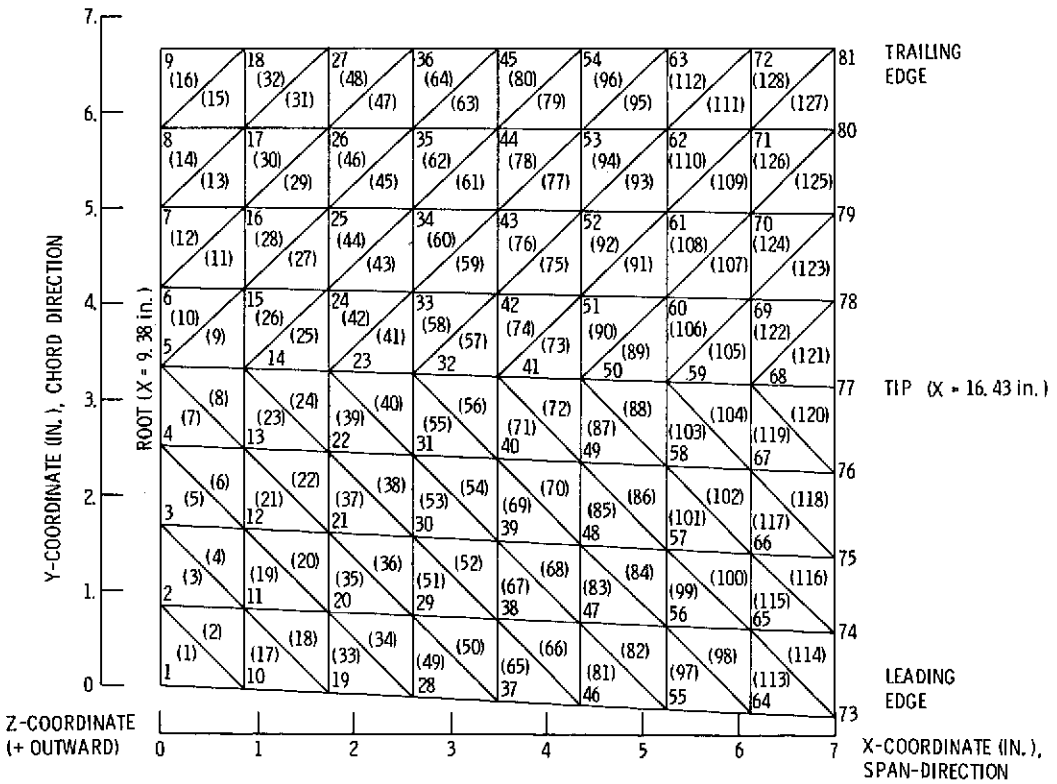

Figure 2. - Projected geometry and finite element representation of airfoil, nodes, and elements (parentheses numbers).

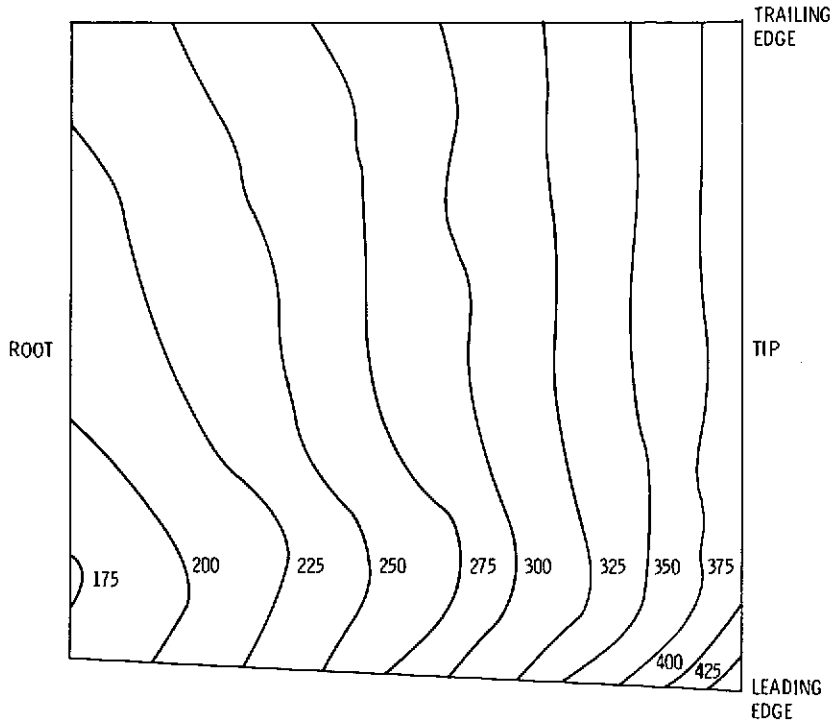

Figure 3. - Airfoil temperature (^{o}F) contour plot as interpolated by pre-processor

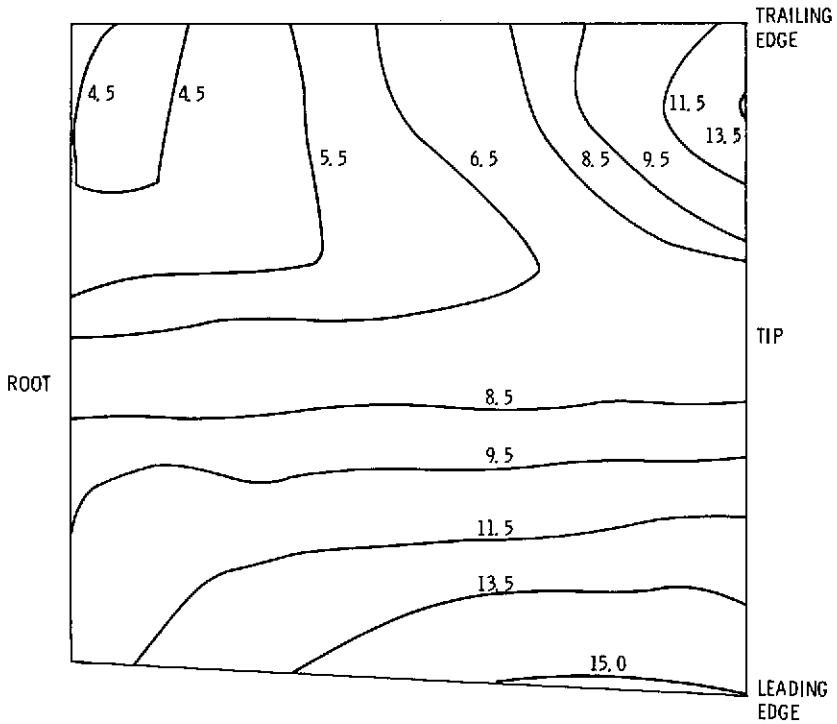

Figure 4. - Airfoil pressure contours (psi) as interpolated by pre-processor.

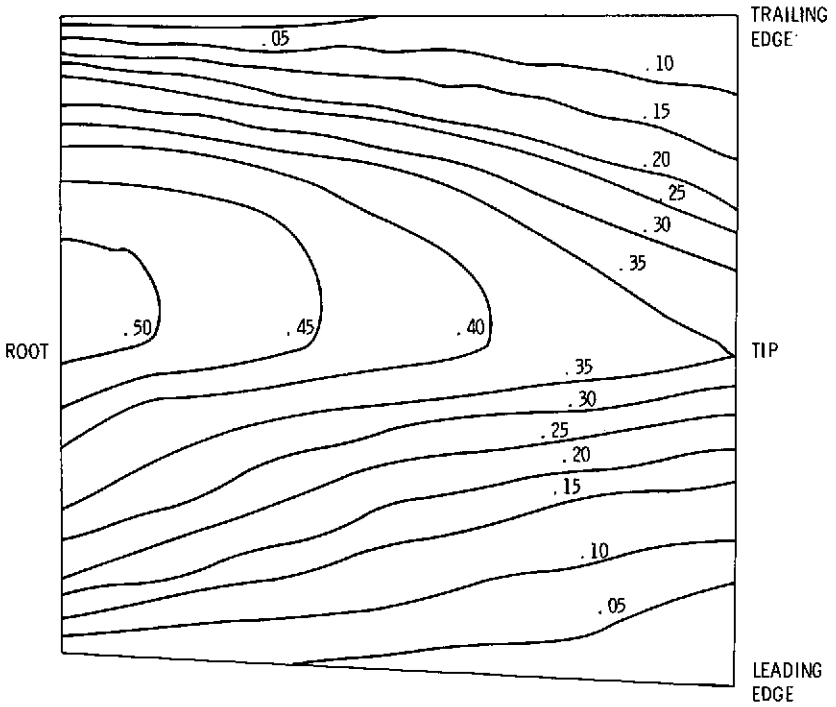

Figure 5. - Airfoil thickness contours (in.) as determined by preprocessor from blade geometry.

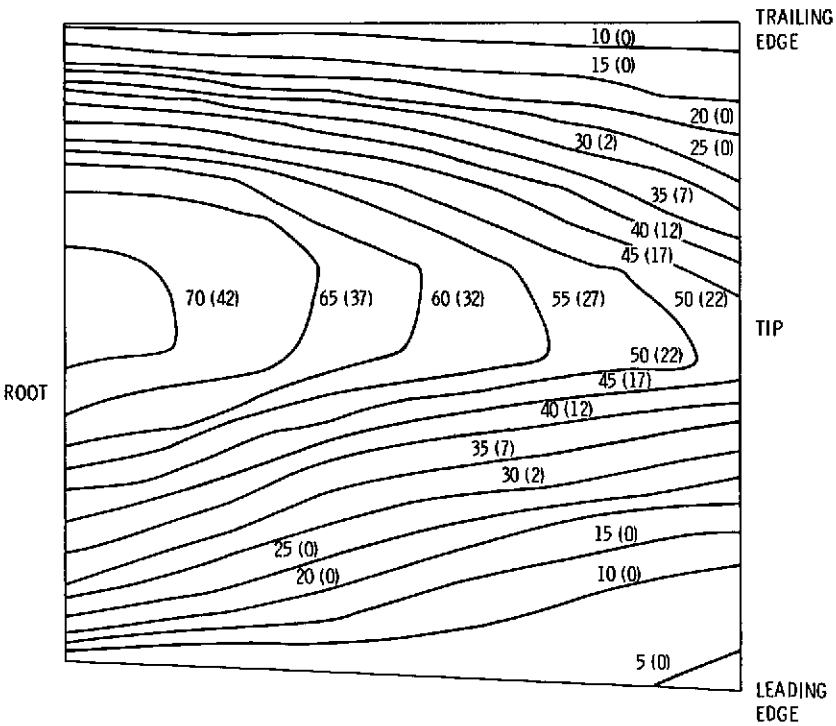

Figure 6. - Airfoil ply contour as determined by pre-processor. Total number of plies and number of plies at 0^0 in parenthesis; difference at $\pm 45^0$ symmetric about mid plane.

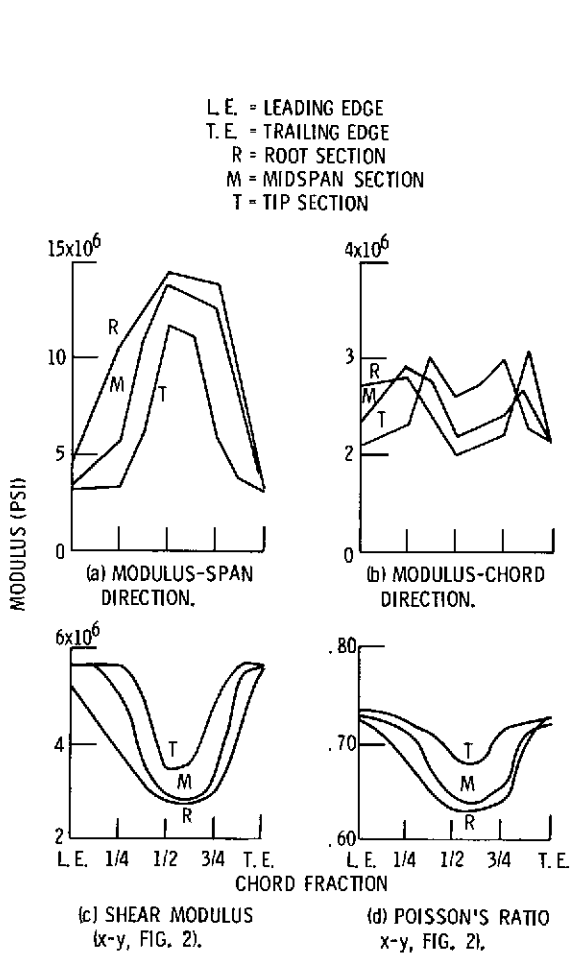

Figure 7. - Airfoil moduli and Poisson's ratio as determined by the pre-processor.

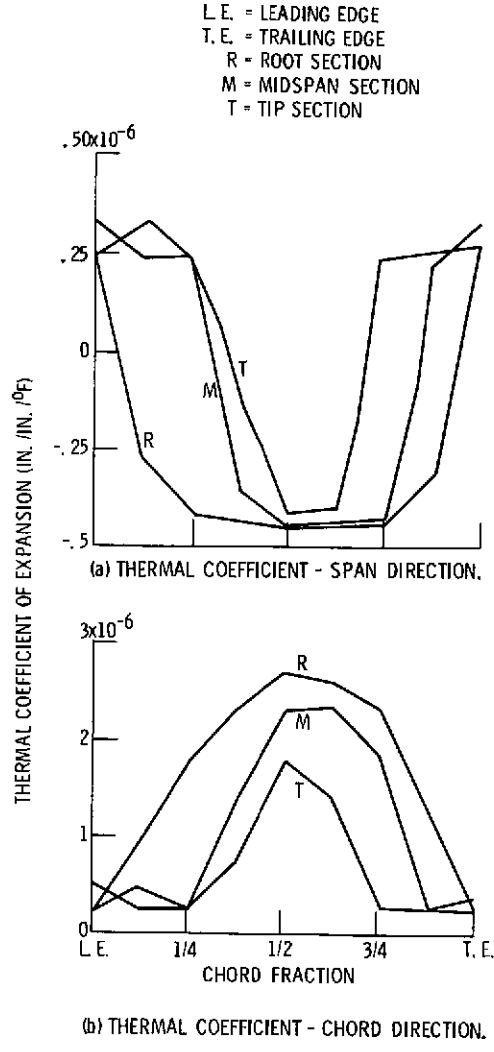

Figure 8. - Airfoil thermal coefficients of expansion as determined by the pre-processor.

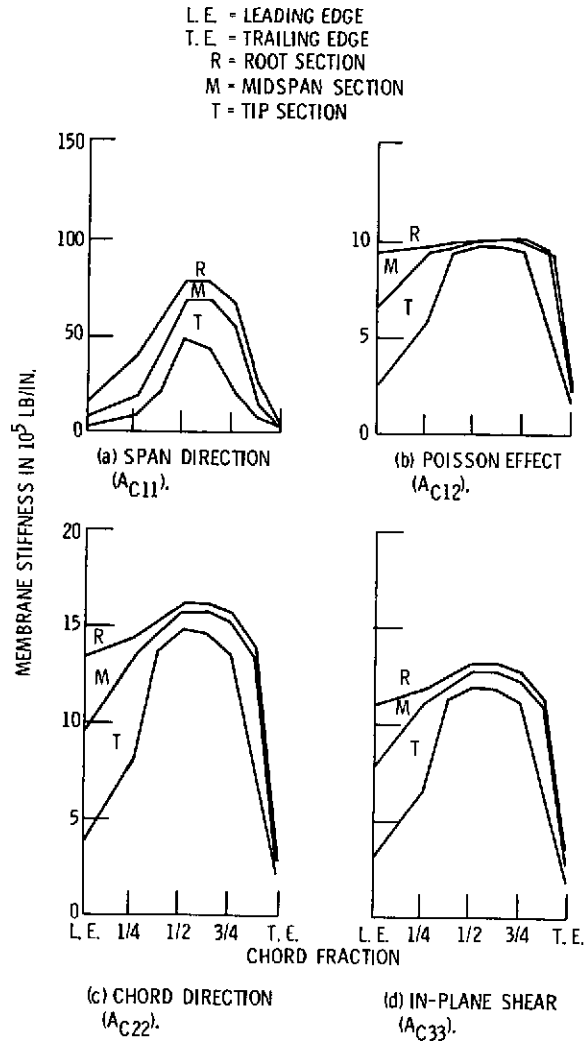

Figure 9. - Airfoil membrane stiffness as determined by the pre-processor.

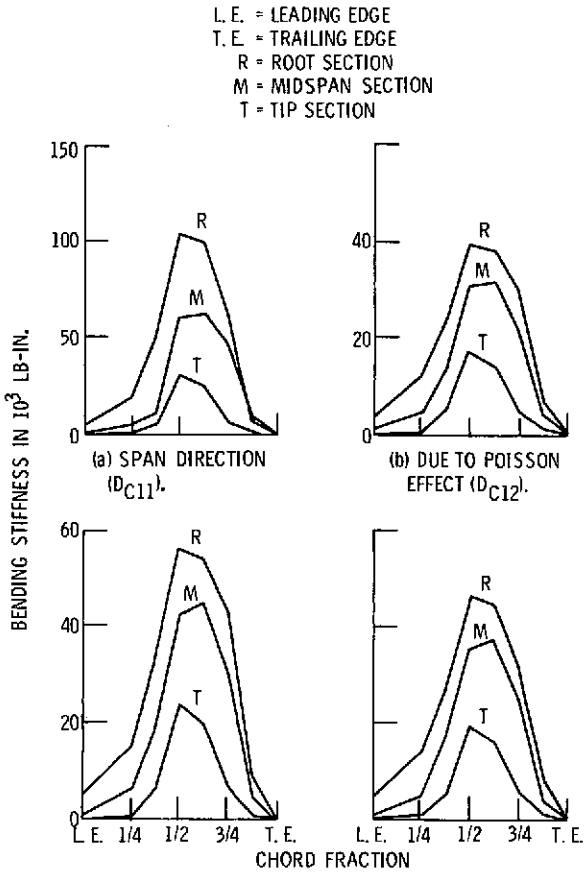

(a) SPAN DIRECTION (D_{C11}).

(b) DUE TO POISSON EFFECT (D_{C12}).

(c) CHORD DIRECTION (D_{C22}).

(d) TORSIONAL (D_{C33}).

Figure 10. - Airfoil bending stiffness as determined by the pre-processor.

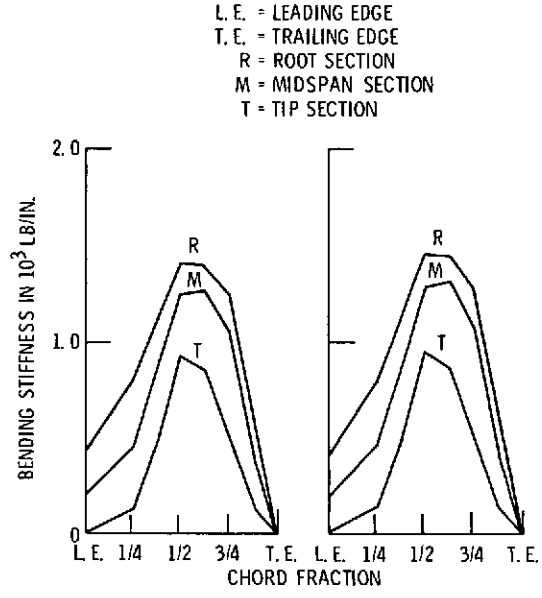

(a) SPAN DIRECTION-BENDING-TWISTING COUPLING (D_{C13}).

(b) CHORD DIRECTION-BENDING-TWISTING COUPLING (D_{C23}).

Figure 11. - Airfoil coupled bending-twisting stiffness as determined by the pre-processor.

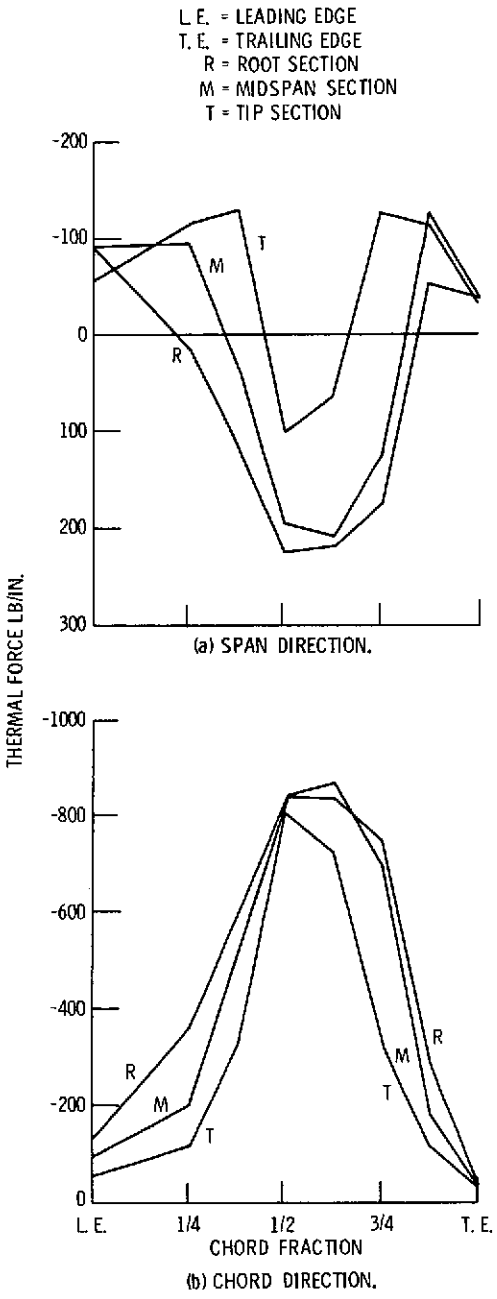

Figure 12. - Airfoil thermal forces as determined by pre-processor due to airfoil temperature shown in figure 2.

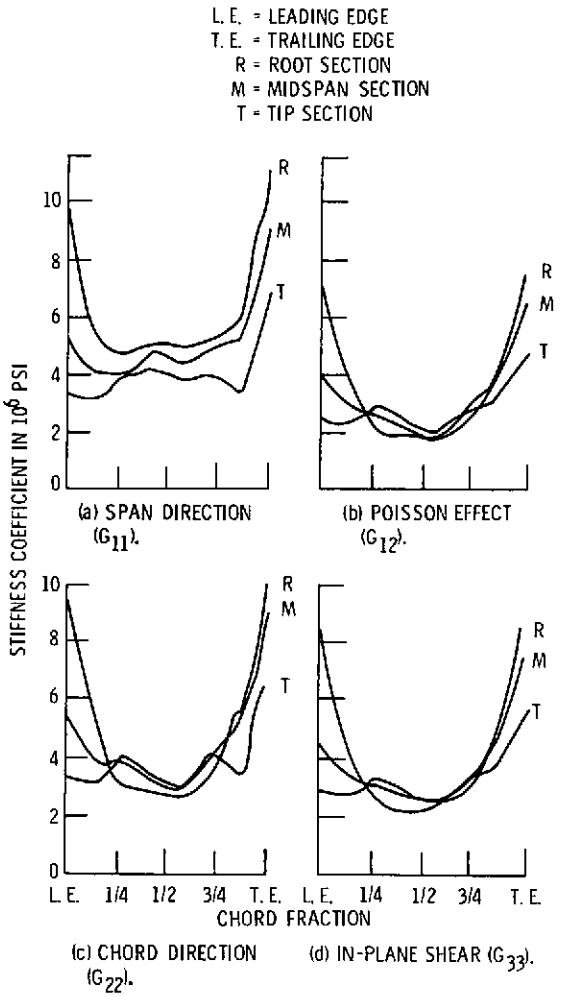

Figure 13. - Plane-stress, stress-strain relationships compatible with CTRIA2 NASTRAN finite element.

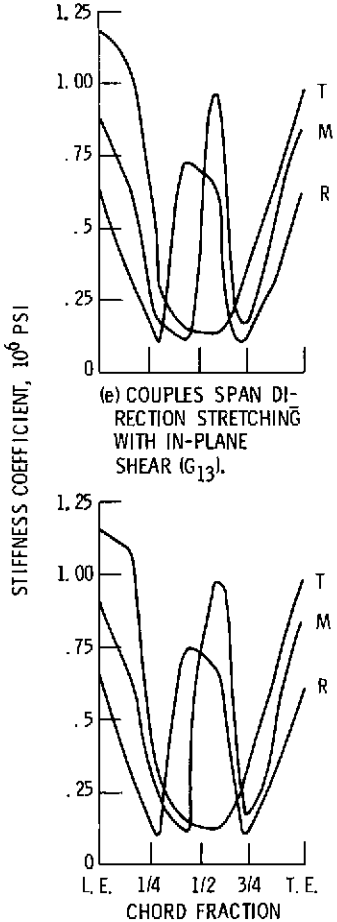

(e) COUPLES SPAN DIRECTION STRETCHING WITH IN-PLANE SHEAR (G_{13}).

(f) COUPLES CHORD DIRECTION STRETCHING WITH IN-PLANE SHEAR (G_{23}).

Figure 13. - Continued.

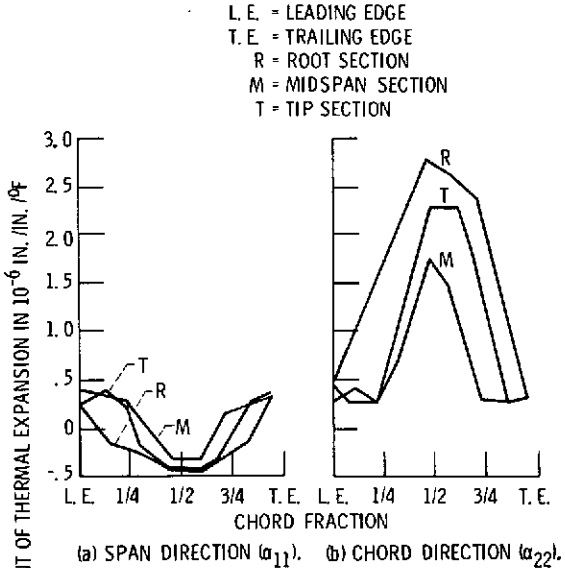

(a) SPAN DIRECTION (α_{11}). (b) CHORD DIRECTION (α_{22}).

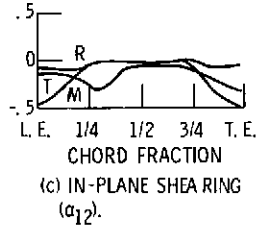

(c) IN-PLANE SHEARING (α_{12}).

Figure 14. - Plane stress thermal coefficients of expansion compatible with the CTRIA2 NASTRAN finite element.

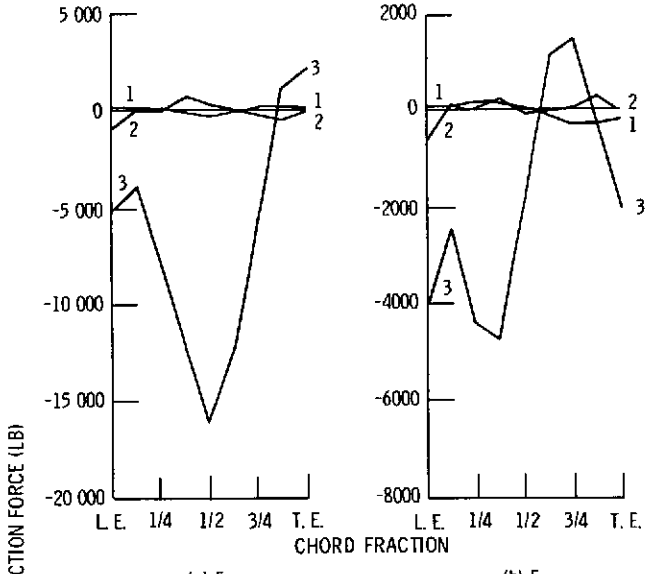

(a) F_x.

(b) F_y.

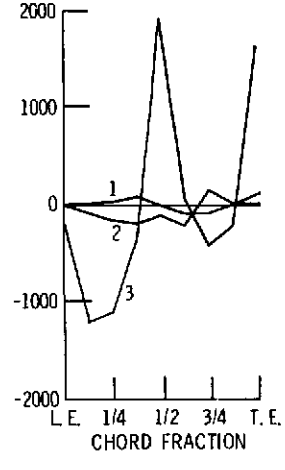

(c) F_z.

LOAD CONDITION: 1. THERMAL; 2. PRESSURE; 3. CENTRIFUGAL

Figure 15. - Root reaction forces vs. blade chord for various load conditions (x, y, z airfoil coordinates, fig. 1).

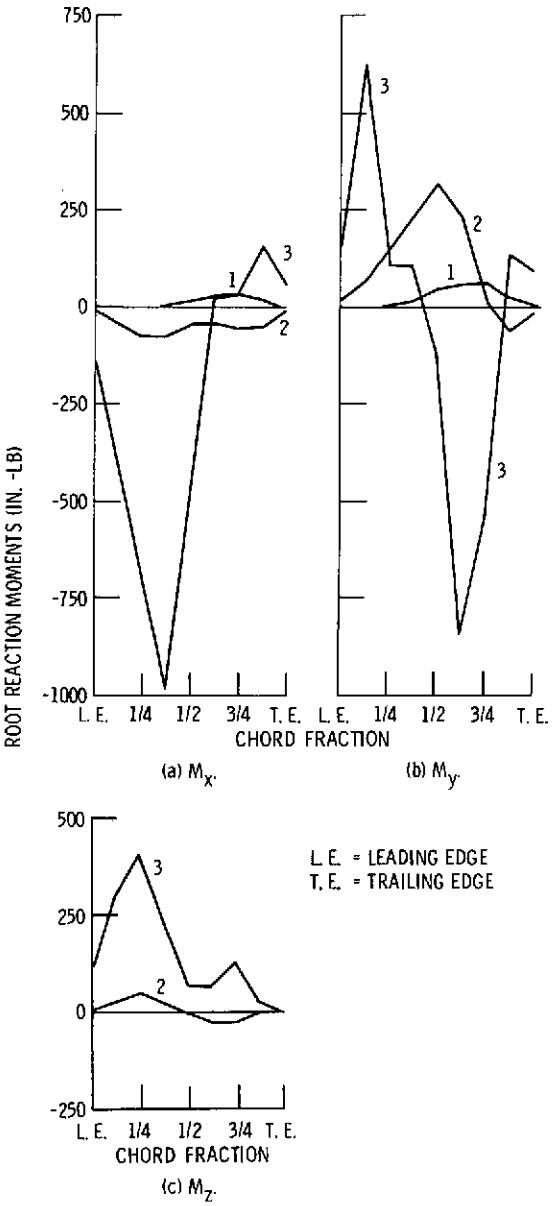

LOAD CONDITION: 1. THERMAL; 2. PRESSURE;
3. CENTRIFUGAL; (COMBINED-
NOT PLOTTED)

Figure 16. - Root reaction moments vs. blade chord for various load conditions (x, y, z airfoil coordinates, fig. 1).

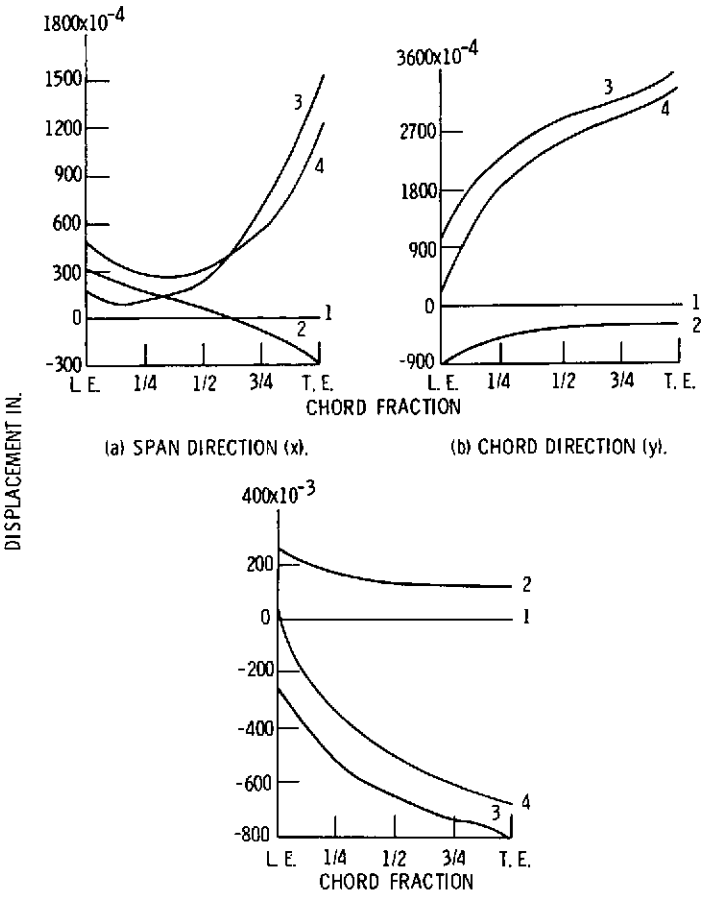

LOAD CONDITION: 1. THERMAL; 2. PRESSURE; 3. CENTRIFUGAL;
4. COMBINED

Figure 17. - Airfoil tip displacements due to various loading conditions.

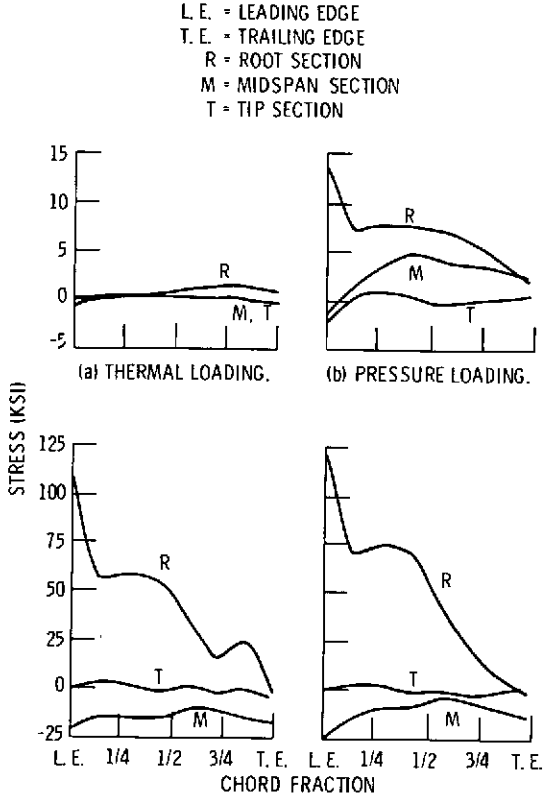

Figure 18. - Span direction stress (σ_{cxx}) due to various loading conditions. Pressure surface.

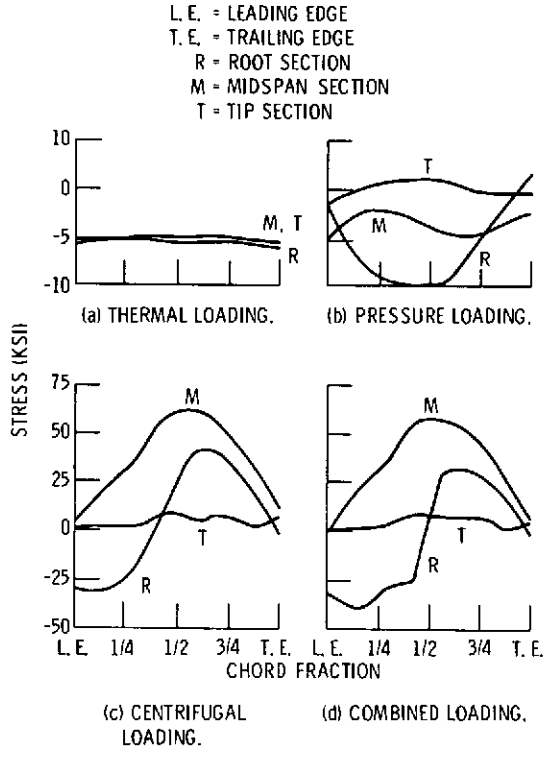

Figure 19. - Span direction stress (σ_{cxx}) due to various loading conditions. Suction surface.

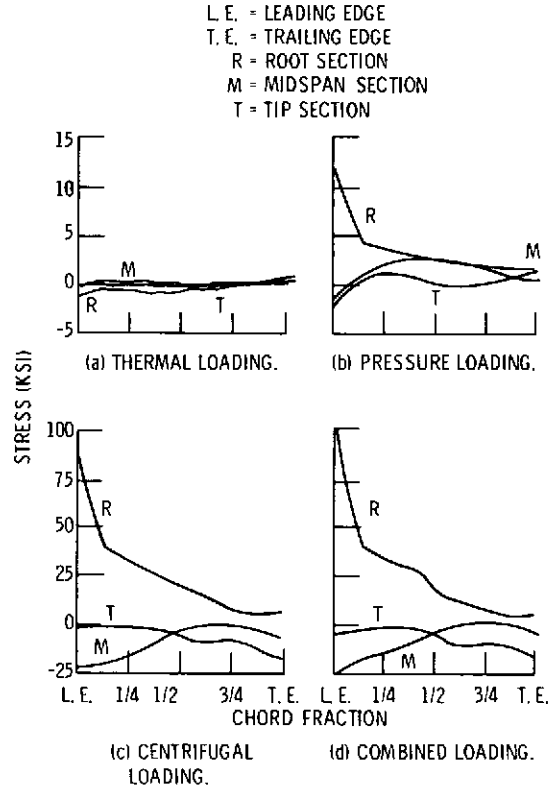

Figure 20. - Chord direction stress (σ_{cyy}) due to various loading conditions. Pressure surface.

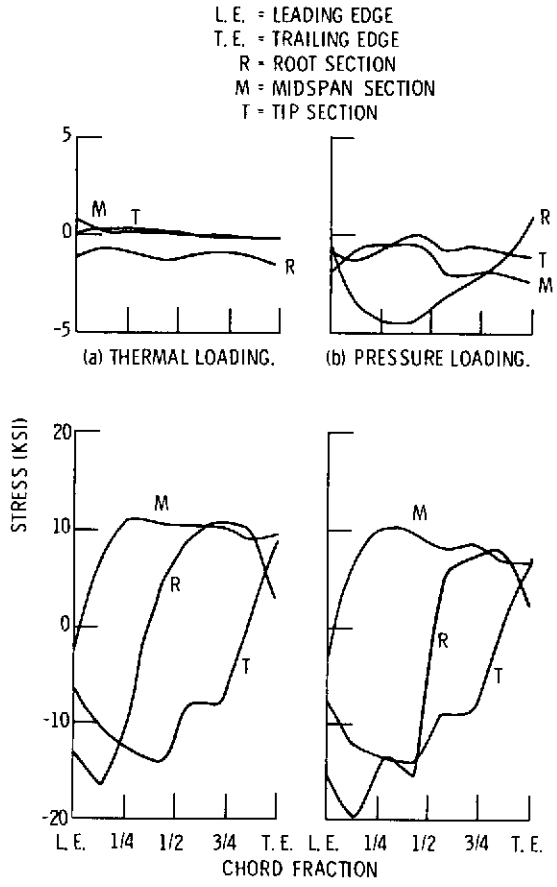

Figure 21. - Chord direction stress (σ_{cyy}) due to various loading conditions. Suction surface.

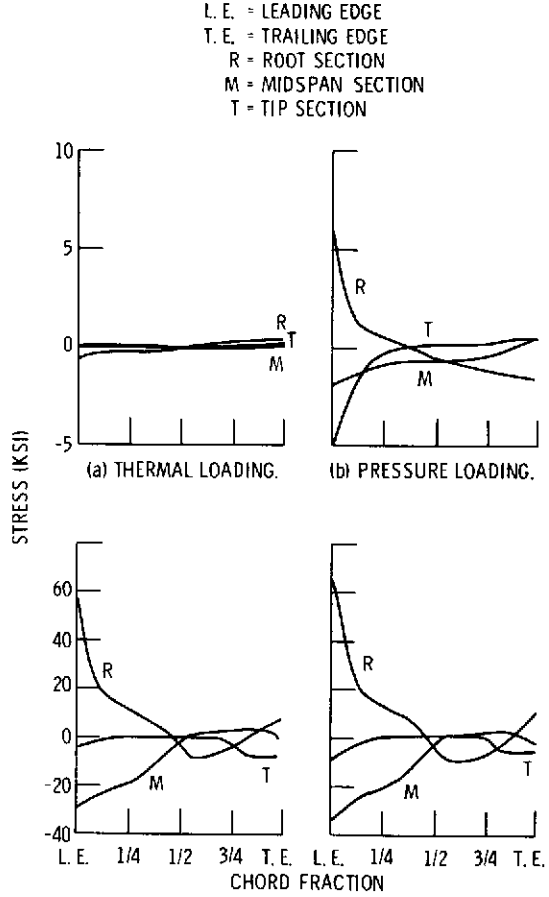

Figure 22. - Shear stress (σ_{cxy}) due to various loading conditions. Pressure surface.

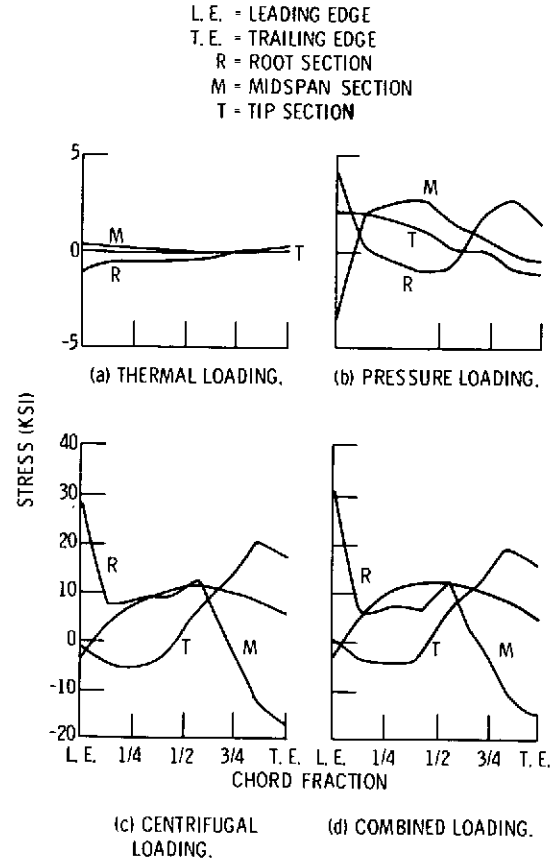

Figure 23. - Shear stress (σ_{cxy}) due to various loading conditions. Suction surface.

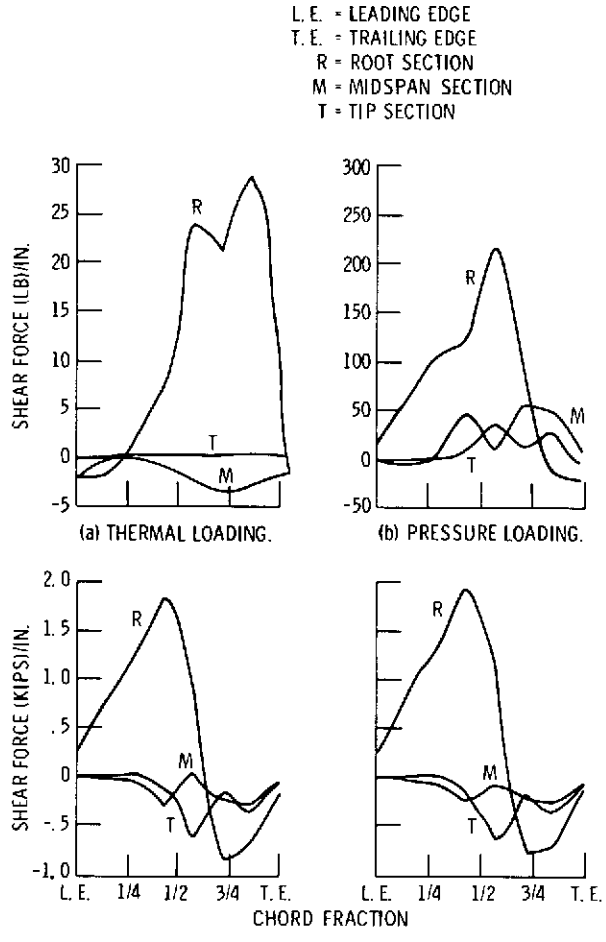

Figure 24. - Through-the-thickness shear force Q_{xz} due to various loading conditions.

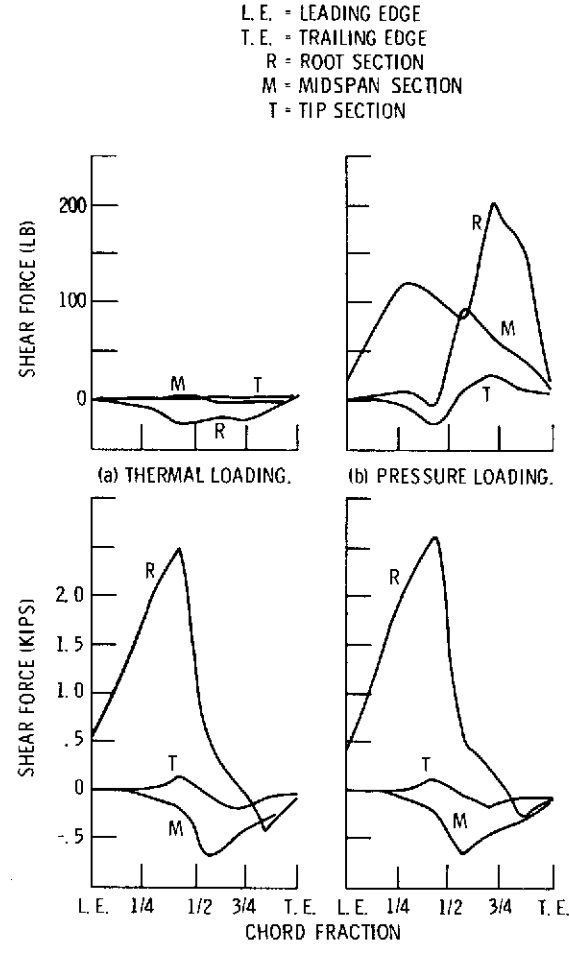

Figure 25. - Through-the-thickness shear force Q_{yz} due to various loading conditions.

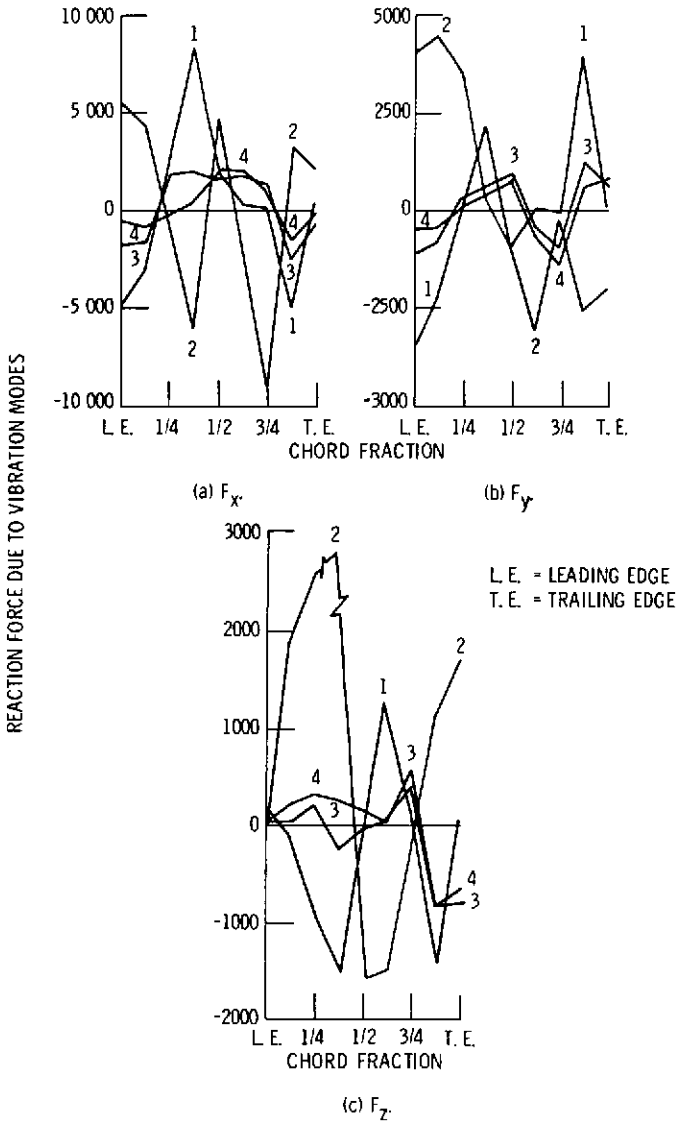

Figure 26. - Root reaction force vs. blade chord for various vibration modes 1, 2, 3, 4 (x, y, z, airfoil coordinates, fig. 1).